

IMPROVED PREDICTION OF SOLUBLE SOLID CONTENT OF APPLE USING A COMBINATION OF SPECTRAL AND TEXTURAL FEATURES OF HYPERSPECTRAL IMAGES**

T. Pang¹, L. Rao¹, X. Chen^{2*}, J. Cheng¹

¹ College of Mechanical and Electrical Engineering at Sichuan Agricultural University, Yaan 625014, China

² College of Information and Engineering at Sichuan Agricultural University, Yaan 625014, China; e-mail: xycheng123@hotmail.com

We established prediction models based on the combination of spectral and different advanced image features to improve the prediction accuracy of solid-soluble content (SSC) of apple. Eight optimal wavelengths were selected using a new variable selection method called variable combination population analysis (VCPA). Image textural features of the first three principal component score images were obtained using a gray level co-occurrence matrix (GLCM) and a local binary pattern (LBP). Next, a random frog algorithm was developed to select optimal textural features for further analysis. A support vector regression (SVR) model based on spectral and different textural features was developed to predict the SSC of the apple. The model based on eight optimal wavelengths and nine optimal GLCM features of principal component images yielded the best result with the determination coefficient for prediction (R_p^2) of 0.9193, root mean square error for prediction (RMSEP) of 0.2955, and the ratio of the standard deviation of the prediction set to the root mean square error of prediction (RPD) with a value of 3.50. These results revealed that the spectral combined with optimal GLCM features from principal component images coupled with the SVR model has the potential for prediction of the SSC of apple.

Keywords: hyperspectral image, soluble solid content, textural feature, VCPA, random frog, SVR.

ОПРЕДЕЛЕНИЕ СОДЕРЖАНИЯ РАСТВОРИМЫХ ТВЕРДЫХ ВЕЩЕСТВ В ЯБЛОКЕ С ИСПОЛЬЗОВАНИЕМ СОЧЕТАНИЯ СПЕКТРАЛЬНЫХ И ТЕКСТУРНЫХ ОСОБЕННОСТЕЙ ГИПЕРСПЕКТРАЛЬНЫХ ИЗОБРАЖЕНИЙ

T. Pang¹, L. Rao¹, X. Chen^{2*}, J. Cheng¹

УДК 535.317.1

¹ Колледж машиностроения и электротехники Сычуаньского сельскохозяйственного университета, Яань 625014, Китай

² Колледж информации и инженерии Сычуаньского сельскохозяйственного университета, Яань 625014, Китай; e-mail: xucheng123@hotmail.com

(Поступила 28 мая 2019)

Созданы модели прогнозирования, основанные на сочетании спектральных и различных расширенных функций изображения для повышения точности прогнозирования твердого растворимого содержимого (SSC) яблока. Восемь оптимальных длин волн выбраны с помощью нового метода выбора переменных — анализа совокупности переменных (VCPA). Текстурные особенности первых трех изображений с оценкой основных компонент получены с использованием матрицы совместной встречаемости уровней серого (GLCM) и локального двоичного шаблона (LBP). Разработан алгоритм случайной лягушки для выбора оптимальных текстурных особенностей для дальнейшего ана-

** Full text is published in JAS V. 87, No. 6 (<http://springer.com/journal/10812>) and in electronic version of ZhPS V. 87, No. 6 (http://www.elibrary.ru/title_about.asp?id=7318; sales@elibrary.ru).

лиза. Для прогнозирования SSC яблока разработана модель регрессии опорных векторов (SVR), основанная на спектральных и текстурных характеристиках. Модель, основанная на восьми оптимальных длинах волн и девяти оптимальных характеристиках GLCM-изображений главных компонент, дает лучший результат с коэффициентом детерминации для прогноза (R_p^2) 0.9193, среднеквадратичной ошибкой прогноза 0.2955 и отношением стандарта. Отклонение прогноза установлено на среднеквадратичную ошибку прогнозирования $RPD = 3.50$. Результаты показывают, что спектр в сочетании с оптимальными характеристиками GLCM из изображений основных компонент в сочетании с моделью SVR имеет потенциал для предсказания SSC яблока.

Ключевые слова: гиперспектральное изображение, растворимое твердое вещество, текстурная характеристика, анализ совокупности переменных, случайная лягушка, модель регрессии опорных векторов.

Introduction. Apple is one of the most popular fruits among consumers worldwide [1, 2]. Soluble solids content (SSC) is one of the most critical fruit quality properties that attract consumers [3, 4]. The traditional methods used for measuring the SSC of the fruits are destructive and time-consuming. Therefore, to meet the requirements of improving product quality in the fruit industry, it is necessary to develop a fast and nondestructive method for detecting the SSC of apple.

Two main methods are used in the field of nondestructive testing of food quality attributes: near-infrared spectroscopy (NIRS) and machine vision [5–7]. NIRS is widely used in the study of internal quality attributes of foods because of its fast and non-invasive nature [8–10]. Owing to the variations in the absorbance of different chemical bonds in the near-infrared range, NIRS can precisely reflect the internal chemical composition of agricultural products. However, it cannot provide spatial information [11]. Machine vision technologies use the image information of the sample surface alone to predict the content of internal components, and the lack of spectral information also limits them.

Hyperspectral imaging (HSI) technology was offered to circumvent these problems [12–16]. This method can provide both spectral and image information and was already employed to detect the internal quality of food. The textural features of the image reflect the intensity changes of pixels and spatial topological relations, which may be related to the chemical composition of SSC in apples. Consequently, a calibration model based on a combination of spectral and textural features may offer more information for predicting SSC than using the spectrum alone.

Many studies have used a combination of image and spectral to combination to predict quality attributes of agricultural products. Examples include prediction of SSC of apple [17], where the best results were obtained with correlation coefficient (R), and root mean square errors of prediction set (RMSEP), with a value of 0.9327 and 0.641%, respectively. Hyperspectral imaging for predicting the moisture content of roasted pistachio kernels established an artificial neural network (ANN) model with results of $R_p^2 = 0.907$ and $RMSEP = 0.179$, respectively [18]. These results indicated that applying a combination of spectral and texture information to predict the SSC of apple is feasible for improving the prediction accuracy in comparison with the use of spectral or texture information alone. Moreover, many previous investigations have shown that the prediction results obtained using texture information alone were unsatisfactory. For example, Liu et al. used the fusion data and the individual textural features to predict the pH in salted meat, and the coefficients of determination (R_p^2) were 0.794 and 0.593, respectively [19]. To reduce the dimensions of hyperspectral images, Cheng et al. extracted textures from the grayscale images at characteristic wavelengths for predicting the K value of pork [20], Jun-Hu Cheng predicted the sensory quality index score of fish fillet using textures extracted from the principal component (PC) score images [21].

Therefore, this study aims to determine the best combination of spectral and two types of textural features (i.e., gray level co-occurrence matrix (GLCM) and local binary pattern (LBP), both extracted from PC images), to obtain a prediction model with the highest efficiency, instead of investigating the modeling results obtained using textures alone. The particular objectives of this study are: (1) to extract spectral data from the region of interest (ROI) of hyperspectral images and select the most prominent spectral bands as optimal spectral bands by VCPA; (2) to extract textural features from PC images using GLCM and LBP, respectively; (3) to select the optimal textural features employing random frog algorithm, and to (4) predict SSC of apple by establishing support vector regression (SVR) model based on optimal spectral alone, optimal spectral information combined with full textural features, full spectral information combined with optimal textural features, and the combination of optimal spectral information and optimal textural features.

Materials and methods. Figure 1 shows a flowchart of the main steps involved in predicting the SSC of apple, where the main process of data analysis was presented in a schematic diagram. Details are presented in subsequent sections.

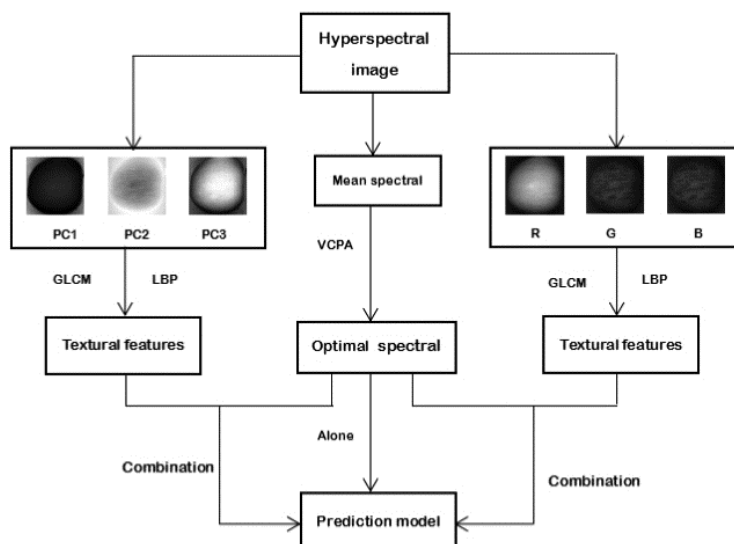


Fig. 1. Flowchart of the prediction of SSC by hyperspectral imaging.

Sample preparation. A total of 126 similarly sized Yantai apples was purchased at the local fruit market in Ya'an, China. The apples were fruit-shaped, and the surface of the fruits was bright and flawless. After washing and labeling, they were placed at standard room temperature for 24 h prior to experiments. All samples were divided into a calibration set and a prediction set, a subset of 90 samples was selected for the calibration set, while the remaining 36 were used for the prediction set.

Hyperspectral images acquisition and calibration. In this study, the hyperspectral imaging system named 'GaiaSorter' (Zolix. Instrument Co. Ltd, China) was used to obtain raw hyperspectral images of apples. The system mainly consisted of a hyperspectral camera with 1344×1024 pixels (Image-λ-V10) covering the spectral range of 387–1034 nm, an illumination unit of 4×200 W tungsten bromide lamps, a translation stage, and a computer with data acquisition software (SpectralView).

The translation stage had a scanning speed of 5 mm/s, the distance between the surface of samples and lens was 255 mm, and the exposure time was set to 11 ms. In order to reduce the effect of dark current of the CCD detector, the raw hyperspectral images (R_{raw}) were calibrated with a white reference image (R_{white}) and a dark reference image (R_{dark}). The white reference image was obtained from whiteboard (~100% reflectance), and the dark reference image was obtained with the lamps off and the camera lens completely covered with its cap (~0% reflectance). The corrected image (R) was calibrated according to the equation:

$$R = \frac{R_{\text{raw}} - R_{\text{dark}}}{R_{\text{white}} - R_{\text{dark}}} \times 100\% . \quad (1)$$

Extraction of spectral information and preprocessing. As apple is a spherical fruit, the lightness on the fruit surface is uneven. Hence, the regions of interest (ROIs) with 60×60 pixels near the center area was manually selected from hyperspectral images of each apple using ENVI 5.1 (ITT Visual Information Solutions, Boulder, CO, USA) software. Then, the mean spectral information of all the pixels within the ROIs was extracted and represented as the spectral value of the sample. Owing to sharp noise in the two sections of 387–400 and 1000–1034 nm (Fig. 2), the whole spectrum was resized to the range of 400–1000 nm with 237 wavebands. Finally, the spectral data were preprocessed using Savitzky-Golay smoothing (the width of the moving window was set to 15, and the polynomial order was 3) and direct orthogonal signal correction (DOSC) [22] with a tolerance value of 1E-3. It is noteworthy that the prediction model can be influenced by the relative values of spectral and textural features. Hence, all input variables were normalized before modeling.

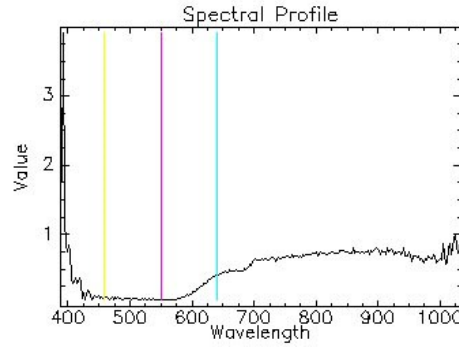


Fig. 2. Original spectrum of pixel points.

Extraction of textural features. Extraction of textural features from images at all wavelengths can produce a large amount of data that may complicate the calculations using the model. To solve the problem of the high dimensionality of hyperspectral images, a principal component analysis was performed in order to transform hyperspectral images into a sequence of principal component score images. In this study, the first three PC images were used to extract textural features as their cumulative variance accounted for $\geq 97\%$ in all.

Extracting textural features using gray level co-occurrence matrix (GLCM). GLCM is a popular statistical texture analysis method [23], which measures the probability that a pixel of a particular gray level occurs at a specified direction and distance from its neighboring pixels [24]. In this study, the GLCM was employed to calculate textural features use four directions ($\theta = 0, 45, 90, \text{ and } 135^\circ$) with the distance between two neighboring pixels equal to 1. As the background could influence the extraction of texture from the whole image, we extracted texture from ROIs of the image. On the other hand, in order to improve the calculation speed and to reduce the impact of noise, the gray levels of images were compressed to 16. The obtained six textural features, namely, maximum probability, contrast, correlation, energy, homogeneity, and entropy, were calculated using the following equations:

$$\text{Maximum probability} = \max \{P(i, j)\}, \quad (2)$$

$$\text{Contrast} = \sum_{i=1}^N \sum_{j=1}^N (i - j)^2 P(i, j), \quad (3)$$

$$\text{Correlation} = \frac{\sum_{i=1}^N \sum_{j=1}^N (ij) P(i, j) - \mu_i \mu_j}{\sigma_i \sigma_j}, \quad (4)$$

$$\text{Energy} = \sum_{i=1}^N \sum_{j=1}^N P(i, j)^2, \quad (5)$$

$$\text{Homogeneity} = \sum_{i=1}^N \sum_{j=1}^N \frac{P(i, j)}{1 + (i - j)^2}, \quad (6)$$

$$\text{Entropy} = - \sum_{i=1}^N \sum_{j=1}^N P(i, j) \lg(P(i, j)), \quad (7)$$

where μ and σ are the means and standard deviations, respectively. Furthermore, i and j represent the row and column in the GLCM. Thus, a textural features matrix of $126 \times 3 \times 24$ (samples \times images \times 6 textural features in four different directions) was obtained in each case. All the textural features were pre-processed using the 15-point SG smoothing mentioned above before developing the prediction models.

Extracting textural features using local binary pattern (LBP). There is a relationship between a pair of pixels in a particular spatial position, where the local binary model can better reflect this space relationship [25, 26]. The basic idea of the LBP is to define a local area (rectangle or circle) and to compare the gray value of the center pixel (g_c) with the gray value of all adjacent pixels (g_h) in an equispaced circular neighborhood of P pixels of radius R . The corresponding binary mode was calculated when $g_c > g_h$ was set to 0 and $g_c < g_h$ was set to 1. Next, the histogram of each cell was calculated and normalized. Finally, the statistical histograms of each cell were connected to obtain the LBP texture features of the image. In the present study, we have applied rotation and uniform invariant of LBP to reduce the dimensions of the LBP patterns, which was expressed by the following formula:

$$U(LBP_{P,R}) = |s(g_{P-1} - g_C) - s(g_0 - g_C)| + \sum_{h=1}^{P-1} |s(g_h - g_C) - s(g_{h-1} - g_C)|, \quad (8)$$

$$LBP_{P,R}^{riu2} = \begin{cases} \sum_{h=0}^{P-1} s(g_h - g_C) & \text{if } U(LBP_{P,R}) \leq 2 \\ P+1 & \text{Otherwise} \end{cases}, \quad (9)$$

where $U(LBP_{P,R})$ are the transitions between 0 and 1; g_C represent the gray value of a pixel at center location, and g_h the gray value of all adjacent pixels in an equispaced circular neighborhood of P pixels in a radius R . The s is a sign function equal to 0 or 1. If $U(LBP_{P,R})$ is higher than 2, the LBP is equal to $P+1$ and regarded as a non-uniform pattern. Ultimately, a total of 10 normalized histogram features of each image was obtained to form a matrix of $126 \times 3 \times 10$ (samples \times images \times features).

SSC reference measurement. After the acquisition of the hyperspectral images of the samples, the physicochemical value of the SSC was measured using a sugar refractometer (LB20T, China). A piece of 2–3 mm flesh was taken from the position which corresponded to the area of spectra acquisition, the appropriate amount of fruit juice was squeezed on the detection prism of the refractometer, and the sample values were recorded. To reduce the effect of the randomness of the measurements, the operation was repeated three times for each sample, and the average value was considered as the main result for sample measurements.

Variable selection method. Usually, a large amount of textural data does not have a positive effect on the prediction accuracy of the model. Therefore, VCPA and random frog algorithms were used to select the optimal variables for spectral and textural features, respectively.

Variable combination population analysis (VCPA). VCPA is a novel variable selection method. It consists of two crucial procedures: (i) the exponentially decreasing function (EDF) was used to determine the ratio of a variable that has to be retained after each run to update the variable space continuously; (ii) a binary matrix sampling (BMS) strategy was used to produce a series of subsets by random combination. The model population analysis was applied to determine the first $\sigma\%$ subsets that have the lowest root mean squares error of cross-validation (RMSECV), followed by computation of the frequency of each variable appearing in those first $\sigma\%$ subsets [27]. The advantage of VCPA is that it provides all variables the same chance to be selected through the BMS strategy. In the present study, the EDF run N was set to 50; the BMS runs times were set to 10000, and the number of variables retained after N times EDF run was set to 14. Finally, the RMSECV of all combinations among these 14 variables was computed, and subsets with the lowest RMSECV were selected. The following formula expresses the ratio of the remaining variables in the i th run of EDF:

$$r_i = e^{-\theta i}, \quad (10)$$

where θ is a constant parameter controlling the curve of EDF. When $i = 0$, all variables are taken for modeling, which indicates that $r_0 = 1$. Furthermore, when $i = N$, $r_N = 14/p$, where p is the number of all variables, θ was calculated as follows:

$$\theta = \frac{\ln(P/14)}{N}. \quad (11)$$

Random frog. Random frog is a variable selection method based on the framework of reversible jump Markov Chain Monte Carlo (RJMCMC) proposed by Li et al. [28, 29]. In quantitative analysis, it is considered the absolute regression coefficient of the variable as the probability of being selected. The higher the probability, the easier is the selection. Briefly, it works in four steps: (1) initialize a subset of variable V_0 consisting of Q variables; (2) propose a candidate subset V^* with Q^* variables; (3) accept V^* as V_1 to replace V_0 with a certain probability; and (4) after N iterations, compute a selection probability of each variable and set a threshold based on experience.

Support vector regression (SVR) analysis. Support vector regression is a frequently used method based on the minimization of structural risk, which can solve the problems of small sample size, nonlinearity, and high dimensionality [30]. The basic idea of SVR is to find an optimal interval that minimizes the error of all training samples from the optimal interval. Similar to the perceptron model, the support vector machine tries to find a straight line in a two-dimensional space to isolate the two types of samples correctly. For a higher dimensional space, a hyperplane with a maximum-margin is necessary. Assuming that the hyperplane can be expressed as $\omega^T x + b = 0$, the distance from the support vector to the optimal hyperplane is $1/\|\omega\|$, so the

maximum-margin is equal to $2/\|\omega\|$. The optimization goal is to minimize the value of $\|\omega\|$. When a function $f = \langle \omega, x \rangle + b$ is used to approximate pairs (x_i, y_i) with $\varepsilon + (\xi_i, \xi_i^*)$ precision, the convex optimization problem can be formalized as

$$\begin{aligned} & \text{Minimize subject to} \\ & \frac{1}{2}\|\omega\|^2 + C\sum_{i=1}^l(\xi_i + \xi_i^*) \\ & \begin{cases} y_i - \langle \omega, x_i \rangle - b \leq \varepsilon + \xi_i \\ \langle \omega, x_i \rangle + b - y_i - b \leq \varepsilon + \xi_i^* \\ \xi_i, \xi_i^* \geq 0 \end{cases} \end{aligned} \tag{12}$$

where $\langle \omega, x \rangle$ denotes the dot product of ω and x , and ε is the maximum biases of y_i and function f that can be tolerated, representing the expectation error. The constant C is the penalty factor, which indicates the degree of punishment for samples that exceed the maximum biases ε . The ξ_i and ξ_i^* are introduced slack variables. After calculating ω and b by constructing a Lagrange function, function f can be written as follows:

$$f(x) = \sum_{i=1}^l(\alpha_i - \alpha_i^*)\langle x_i, x \rangle + b, \tag{13}$$

where α_i and α_i^* are Lagrange multipliers, l is the number of samples in the calibration set, and x_i, x denotes the dot product of x_i and x .

The radial basis function (RBF) was used as a kernel function to map training data into some feature space and then apply a standard SVR algorithm; moreover, the present study employed the grid method and 5-fold cross-validation to determine the optimal penalty factor (C) and the parameter of kernel function (γ).

Model evaluation. The model evaluation parameters include the determination coefficient for calibration (R_c^2) and the determination coefficient for prediction (R_p^2), the root mean square error of calibration (RMSEC) and the root mean square error of prediction (RMSEP), and the ratio of the standard deviation of prediction set to the root mean square error of prediction (RPD). Generally, the values of R_c^2 and R_p^2 are in the range of 0–1, and a well-performing model should have a high value of R_c^2, R_p^2 , and RPD and low values of RMSEC and RMSEP. RPD values higher than 2.0 indicate that the model has decent predictive performance, whereas RPD values above 3.0 indicate good to excellent prediction accuracy [31, 32].

Results and discussion. *Statistics of SSC of samples.* To ensure that the information from the calibration set used to establish the predictive model is representative, the Kennard-Stone method was used to divide the 126 samples into two groups, the calibration set and the prediction set. The statistics of SSC of apples in the calibration and the prediction are shown in Table 1. The range of the calibration set is 12–17.75 and covers the range of the prediction set. The mean value and the standard deviation of the calibration set are 14.6367 and 1.1738, respectively.

TABLE 1. Statistics for the SSC Values of the Calibration Set and Prediction Set

	Number of samples	Min	Max	Mean	Std
Total	126	12.0000	17.7500	14.6579	1.1041
Calibration set	90	12.0000	17.7500	14.6367	1.1738
Prediction set	36	12.9000	17.2500	14.7111	0.9196

Modeling based on spectral information. Before the selection of effective variables, the performance of the full-spectrum SVR model was investigated. When the SVR algorithm was involved in building a predictive model, the optimal penalty factor (c) and the parameter of kernel function (γ) were achieved with $c = 16$ and $\gamma = 9.765 \times 10^{-4}$, respectively. As can be observed in Table 2, the model yielded a result with $R_p^2 = 0.6357$, RMSEP = 0.5799, and RPD = 1.51 for SSC prediction. The value of RPD and R_p^2 indicates that the generalization ability of the model at the present stage is insufficient.

TABLE 2. Performance of SVR Model Based on Spectral Features Alone

Method	Number of variables	Calibration		Prediction		
		R_c^2	RMSEC	R_p^2	RMSEP	RPD
Full spectral	237	0.9306	0.3156	0.6357	0.5799	1.51
VCPA	8	0.9185	0.3347	0.7881	0.4225	2.18
random frog	10	0.9029	0.3771	0.7960	0.3622	2.25

The VCPA was implemented to select eight optimal wavelengths (411, 427, 447, 449, 452, 576, 621, and 944 nm) from the full spectra, and the frequency of selected variables after EDF runs is presented in Fig. 3. The selected optimal variable at 944 nm was likely due to the combined effect of water and carbohydrate absorbance. Furthermore, chlorophylls associated with fruit maturity have absorption bands occurring at about 621 and 576 nm [33, 34]. From 400 to 500 nm, there is an increase in absorbance, with a stronger peak at about 490 nm. Although the results of chemical property analysis of spectral features from 400 to 500 nm are unclear, the results showed that this region may be related to the SSC prediction. The calibration model was developed based on the eight optimal wavelengths coupled with the SVR algorithm. As it can be seen in Table 2, the results of the SVR model based on the optimal wavelengths ($R_c^2 = 0.9185$, RMSEC = 0.3347, $R_p^2 = 0.7881$, RMSEP = 0.4225, and RPD = 2.18) show considerable progress compared to the full-spectrum. However, the results are not entirely satisfactory, and the information used for modeling may not be sufficiently rich.

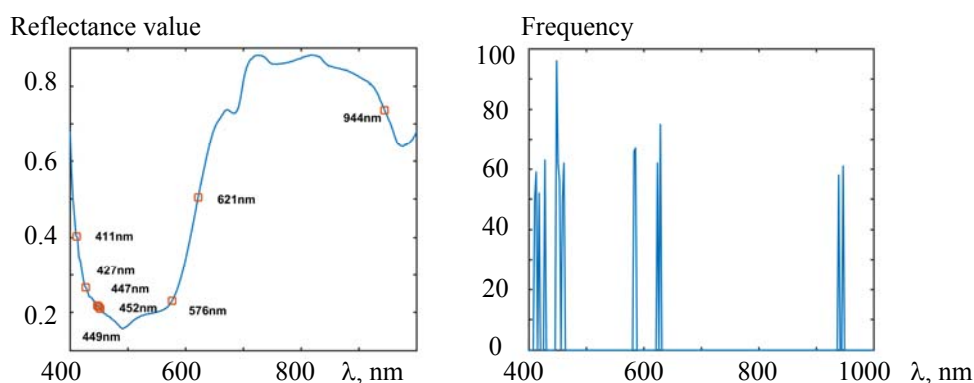


Fig. 3. Selected variables and the frequency of selected variables within 50 times by VCPA.

The random frog algorithm is used to calculate the probability of all wavelengths being selected, and then the largest top 10 (404, 421, 428, 442, 445, 447, 567, 604, 607, and 960 nm) are selected as the optimal variables. Taking these optimal variables as the input of the SVR model, the prediction model finally resulted in $R_c^2 = 0.9029$, RMSEC = 0.3771, $R_p^2 = 0.7960$, RMSEP = 0.3622, and RPD = 2.25. As shown in Table 2, the model established with the variables selected by the random frog algorithm achieved results similar to those obtained with the VCPA algorithm.

Modeling based on the combination of spectral selected by VCPA and textural features. To compensate for the drawbacks of using spectral data alone, the SVR model was constructed depending on the combination of spectral and textures extracted from PC images. In Table 3, the model evaluation parameters of the model ($R_p^2 = 0.8437$, RMSEP = 0.4682, and RPD = 2.14) based on the combination of spectral and full GLCM features were compared with the model that used spectral data alone. The R_p^2 value improved by 7.05%, although the RMSEP value increased by 10.82%. For LBP features, the model ($R_p^2 = 0.8439$, RMSEP = 0.3853, and RPD = 2.38) based on spectral combined full features showed some progress.

According to the statistical analysis of the results mentioned above, for the predictive ability of SSC, it can be observed that although the performance of the model based on spectral information and full textural features has been improved, it is still not satisfactory. We supposed that this might be because of the fusion of textural features and spectral data, which results in data redundancy. Therefore, the textural feature was selected using the random frog algorithm. The more important a textural feature is, the more likely it is to be selected into the optimal subsets. We set the threshold to 0.15 based on experience and selected nine optimal features for GLCM features (maximum probability $_{\theta=0^\circ}$ located on PC1 image, energy $_{\theta=0^\circ}$, homogeneity $_{\theta=0^\circ}$, entropy $_{\theta=90^\circ}$, maximum probability $_{\theta=135^\circ}$ located on PC2 image, correlation $_{\theta=0^\circ}$, homogeneity $_{\theta=0^\circ}$, contrast $_{\theta=135^\circ}$,

and correlation_{θ=135°} located on the image PC3). For LBP features, we also set the threshold to 0.15 and select 8 optimal features. Table 3 shows that the performance of the model based on a combination of spectral and optimal GLCM features ($R_c^2 = 0.9330$, RMSEC = 0.2909, $R_p^2 = 0.9193$, RMSEP = 0.2955, and RPD = 3.50) and the model based on spectral combined with optimal LBP features ($R_p^2 = 0.9121$, RMSEC = 0.3131, $R_p^2 = 0.8740$, RMSEP = 0.4392, and RPD = 2.81) were more efficient than those based on spectral information plus complete textural features. Specifically, the model using spectral and optimal GLCM features performed better than the model using spectral and optimal LBP features. The measured and predicted values of the different models are collected in Fig. 4.

TABLE 3. Performance of SVR Model Based on Spectral and Different Textural Features

Index	Data set	Number of variables	Calibration		Prediction		
			R_c^2	RMSEC	R_p^2	RMSEP	RPD
Optimal spectral+ full textures	Spectral+GLCM	8+72	0.8924	0.3595	0.8437	0.4682	2.14
	Spectral+LBP	8+30	0.9111	0.3486	0.8439	0.3853	2.38
VCPA	Spectral+GLCM	8+9	0.9330	0.2909	0.9193	0.2955	3.50
	Spectral+LBP	8+8	0.9121	0.3131	0.8740	0.4392	2.81

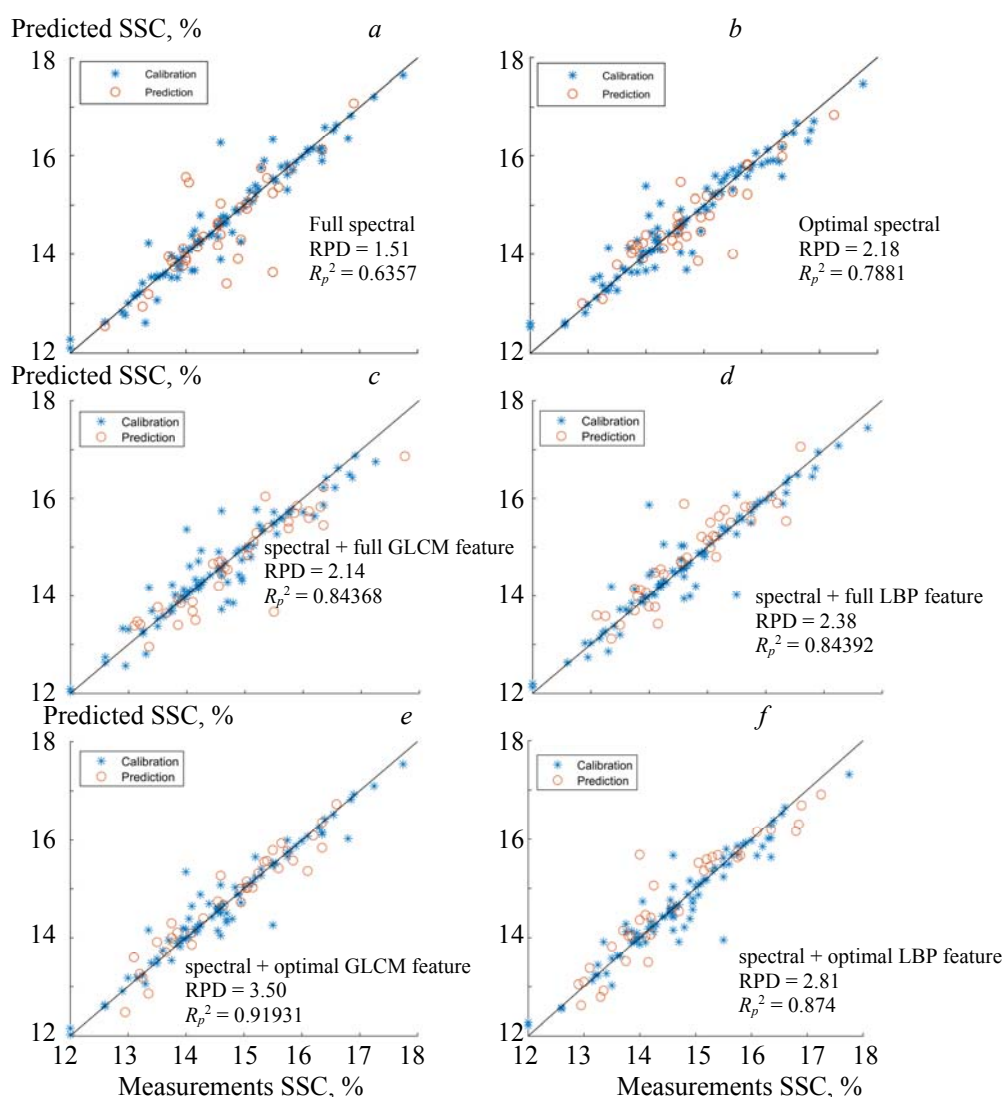


Fig. 4. Measured vs. predicted SSC for model based on different combinations of spectral and textures of PC images. Spectral alone (a), (b), and combinations (c)–(f).

Modeling based on combination of spectral selected by random frog and textures. Similar to the previous section, in order to verify that there is redundancy in the full texture feature data, the optimal spectral features were combined with the full texture features to establish a prediction model. The as-obtained results are in line with expectations. Whether the spectrum is combined with full GLCM or LBP features, the model prediction results only show a small increase or even a regression. Moreover, prediction models based on full-spectrum and optimal texture features were established. The model based on full spectral and optimal GLCM texture features gave the results $R_p^2 = 0.8359$, RMSEP = 0.3417, and RPD = 2.34. Furthermore, the model based on full spectral and optimal LBP texture features gave the results $R_p^2 = 0.8467$, RMSEP = 0.3331, and RPD = 2.48. In the next step, the optimal spectrum was combined with the texture features optimized by the random frog algorithm to establish an improved SVR model. As shown in Table 4, the predicted results of the model based on optimal spectral and GLCM textures are $R_p^2 = 0.8406$, RMSEP = 0.3414, and RPD = 2.52, and the results of the model based on optimal spectral and LBP textures are $R_p^2 = 0.8892$, RMSEP = 0.3324, and RPD = 3.05. Thus, it can be concluded that after the optimization of the full textural features, the performance of the model was significantly improved.

TABLE 4. Performance of SVR Model Based on Spectral and Different Textural Features

Index	Data set	Number of variables	Calibration		Prediction		
			R_c^2	MSEC	R_p^2	RMSEP	RPD
Optimal spectral +full textures	Spectral+GLCM	10+72	0.9176	0.3417	0.7104	0.5024	1.65
	Spectral+LBP	10+30	0.8916	0.3968	0.8236	0.3816	2.13
Full spectral+ optimal texture	Spectral+GLCM	237+9	0.9228	0.3223	0.8359	0.3417	2.34
Full spectral+optimal texture	Spectral+LBP	237+8	0.9497	0.2481	0.8467	0.3331	2.48
Random frog	Spectral+GLCM	10+9	0.9455	0.2769	0.8406	0.3414	2.52
	Spectral+LBP	10+8	0.8998	0.3591	0.8892	0.3324	3.05

Conclusions. The present study explored the feasibility of using optimal wavelengths integrated with textural features to develop a simple and efficient prediction model for SSC detection. Using VCPA and the random frog algorithm to select eight and 10 optimal wavelengths, respectively, and building a simplified model separately gave results that were not satisfactory. The predictive ability of the model obtained by fusing spectral and textural features was better. For instance, the model based on the fusion of full spectral and optimal LBP features had values of R_p^2 of 0.8467, RMSEP of 0.3331, and RPD of 2.48. Furthermore, we used the random frog algorithm to select optimal textural features for further analysis. The results show that the performance of the model ($R_p^2 = 0.9193$, RMSEP = 0.2955, and RPD = 3.50) based on the combination of optimal spectral and optimal textures of GLCM was best.

Acknowledgements. The authors are grateful to Sichuan Province Department of Education (China) for support through the program of “Research on Apple Quality Nondestructive Testing Method Based on Hyperspectral Image Technology” (17ZB0333). This work was also supported by the Lab of Agricultural Information Engineering, Sichuan Key Laboratory. This study was funded by Natural Science Program of Sichuan Education Department (17ZB0333).

Ethical approval. This article does not contain any studies with human participants or animals.

REFERENCES

1. W. Huang, L. Chen, J. Li, Z. Guo, Determination of Soluble Solids Content in Apple using Hyperspectral Imaging and Variable Selection Algorithms, Conference in Kansas City, Missouri, July 21–24, 2013 (2013), doi: 10.13031/aim.20131620975.
2. J. Dong, W. Guo, *Food Anal. Methods*, **8**, No. 10, 2635–2646 (2015).
3. F. Mendoza, R. Lu, D. Ariana, H. Cen, B. Bailey, *Postharvest. Biol. Technol.*, **62**, No. 2, 149–160 (2011).
4. J. Dong, W. Guo, Z. Wang, D. Liu, F. Zhao, *Food Anal. Methods*, **9**, No. 5 (2016).
5. D. J. Lee, R. Schoenberger, J. Archibald, S. McCollum, *J. Food Eng.*, **86**, 388–398 (2008).
6. S. N. Jha, K. Narsaiah, A. D. Sharma, M. Singh, S. Bansal, R. Kumar, *JFST*, **47**, No. 1, 1–14 (2010).
7. L. Yang, F. Yang, N. Noguchi, *IFAC Proc.*, **18**, 14145–14150 (2011).

8. Z. Xiaobo, Z. Jiewen, H. Xingyi, L. Yanxiao, *Chemometr. Intell. Lab.*, **87**, 69–77 (2007).
9. H. Zhang, X. Sun, Y. Liu, T. Liu, A. Ouyang, Y. Pan, et al. *Tran. Chin. Soc. Agric. Eng.*, **25**, 340–344 (2009).
10. D. Yang, D. He, A. Lu, D. Ren, J. Wang, *Infrared Phys. Technol.*, **83**, 206–216 (2017).
11. M. Huang, Q. Wang, M. Zhang, Q. Zhu, *J. Food Eng.*, **128**, 24–30 (2014).
12. P. Rajkumar, N. Wang, G. Eimasry, G. S. V. Raghavan, Y. Garipey, *J. Food Eng.*, **108**, No. 1, 194–200 (2012).
13. H. Cen, R. Lu, Q. Zhu, F. Mendoza, *Postharvest Biol. Technol.*, **111**, 352–361 (2016).
14. A. López-Maestresalas, J. C. Keresztes, M. Goodarzi, S. Arazuri, C. Jarén, W. Saeys, *Food Control*, **70**, 229–241 (2016).
15. S. Suktanarak, S. Teerachaichayut, *J. Food Eng.*, **215**, 97–103 (2017).
16. T. Guo, M. Huang, Q. Zhu, Y. Guo, J. Qin, *J. Food Eng.*, **218**, 61–68 (2017).
17. Sh. Fan, B. Zhang, J. Liu, *Postharvest Biol. Technol.*, **121**, 51–61 (2016).
18. T. Mohammadi-Moghaddam, S. M. A. Razavi, M. Taghizadeh, B. Pradhan, A. Sazgarnia, A. Shaker-Ardekani, *J. Food Meas. Charact.* (2018).
19. D. Liu, H. Pu, D. W. Sun, L. Wang, X. A. Zeng, *Food Chem.*, **160**, 330–337 (2014).
20. W. Cheng, D. W. Sun, H. Pu, Y. Liu, *LWT-Food Sci. Technol.*, **72**, 322–329 (2016).
21. J. H. Cheng, D. W. Sun, *LWT-Food Sci. Technol.*, **63**, 892–898 (2015).
22. J. A. Westerhuis, S. D. Jong, A. K. Smilde, *Chemometr. Intell. Lab.*, **56**, No. 1, 13–25 (2001).
23. D. A. Clausi, *Can. J. Remote Sens.*, **28**, 45–62 (2002).
24. X. Li, P. Nie, Z. J. Qiu, Y. He, *Expert. Syst. Appl.*, **38**, 11149–11159 (2011).
25. S. Nigam, A. Khare, *Multimed. Tools Appl.*, **75**, 17303–17332 (2016).
26. T. Tang, L. Dai, Z. Yin, Abstr. 5th Int. Conf. Mechatronics, Materials, Chemistry and Computer Engineering, 6 (2017)
27. Y. H. Yun, W. T. Wang, B. C. Deng, G. B. Lai, X. B. Liu, D. B. Ren, *Anal. Chim. Acta*, **862**, 14–23 (2015).
28. H. D. Li, Q. S. Xu, Y. Z. Liang, *Anal. Chim. Acta*, **740**, 20–26 (2012).
29. Y. H. Yun, H. D. Li, L. R. Leslie, *Spectrochim. Acta A*, **111**, 31–36 (2013).
30. U. Thissen, M. Pepers, B. Üstün, W. J. Melssen, L. M. Buydens, *Chemometr. Intell. Lab.*, **73**, No. 2, 169–179 (2004).
31. S. Fan, W. Huang, Z. Guo, *Food Anal. Methods*, **8**, No. 8, 1936–1946 (2015).
32. X. L. Chu, *Molecular Spectroscopy Analytical Technology Combined with Chemometrics and Its Applications*, Beijing, Chemical Industry Press, 86–88 (2011).
33. V. A. Mcglone, S. Kawano, *Postharvest Biol. Technol.*, **13**, No. 2, 131–141 (1998).
34. R. Lu, *Postharvest Biol. Technol.*, **31**, No. 2, 147–157 (2004).